Check for updates

The FASEB Journal

FASEB
Federation of American Societies for Experimental Biology

RESEARCH ARTICLE

Ufl1-Mediated UFMylation Sustains Amelogenesis by Stabilizing RUNX2

Da Liu[1] | Lin Chen[1] | Huning Xu[2] | Xueqin Yang[1] | Ke Wang[2] | Miao Wang[2] | Xiao-Jing Zhu[1]

[1]Zhejiang Key Laboratory of Organ Development and Regeneration, College of Life and Environmental Sciences, Hangzhou Normal University, Hangzhou, Zhejiang, China | [2]Key Laboratory of Aging and Cancer Biology of Zhejiang Province, Zhejiang Key Laboratory of Medical Epigenetics, School of Basic Medical Sciences, Hangzhou Normal University, Hangzhou, Zhejiang, China

Correspondence: Xiao-Jing Zhu (xiao_jingzhu@hznu.edu.cn) | Miao Wang (mwanghznu@126.com)

Received: 17 March 2026 | **Revised:** 22 June 2026 | **Accepted:** 1 July 2026

Keywords: Ameloblasts | Amelogenesis Imperfecta | dental enamel | gene deletion | protein stability | tooth development

ABSTRACT

UFMylation is a conserved ubiquitin-like post-translational modification that controls protein stability and tissue homeostasis, while its role in amelogenesis remains largely uncharacterized. Here, we investigated the function of UFL1, the sole E3 ligase of the UFMylation pathway, in mammalian enamel development using *K14-Cre*-mediated epithelial-specific *Ufl1* knockout mice. *Ufl1* ablation caused severe amelogenesis imperfecta, with impaired enamel deposition, hypomineralization, and progressive tooth damage, accompanied by abnormal cervical loop development. Transcriptomic profiling revealed elevated endoplasmic reticulum stress and dysregulated expression of enamel mineralization genes, including significant downregulation of downstream targets of RUNX2, a master regulator of amelogenesis. We further demonstrated that UFL1 and DDRGK1 directly interacted with RUNX2, and UFL1-mediated UFMylation stabilized RUNX2 protein at the post-translational level. Taken together, this study identifies a novel UFMylation-RUNX2 regulatory axis essential for amelogenesis, providing new mechanistic insights into amelogenesis imperfecta and potential therapeutic targets for dental enamel defects.

1 | Introduction

Ubiquitin and ubiquitin-like (UBL) modifications represent a class of post-translational modifications that play pivotal regulatory roles in numerous cellular processes. By modulating the protein–protein interactions and stability of their target proteins, these UBL modifications govern proteomic complexity and functional homeostasis [1]. Among them, UFMylation is highly conserved across nearly all eukaryotic organisms, with its regulatory network participating in diverse biological processes including hematopoiesis, the endoplasmic reticulum (ER) stress response, the unfolded protein response, and the DNA damage response [1, 2].

The UFMylation pathway exerts regulatory effects on substrate functions through the covalent conjugation of ubiquitin fold modifier 1 (UFM1) to target proteins [3]. It is a reversible post-translational modification that relies on a simple enzymatic cascade consisting of the E1 enzyme UBA5, E2 enzyme UFC1, and the sole E3 ligase UFL1, together with two UFM1-specific proteases (UFSP1 and UFSP2) that mediate deUFMylation [1]. During the UFMylation process, UFL1 mediates the covalent attachment of the ubiquitin-like modifier UFM1 to lysine residues on target proteins, a process that requires the structural complementarity between UFL1 and DDRGK1 [1, 2].

Mutations or loss-of-function of UFMylation pathway components are highly associated with various human disorders and multiple mouse developmental abnormalities [1, 2, 4]. Specifically, mutations in *UFM1*, *UBA5*, and *UFC1* are linked to early-onset encephalopathy and defective brain development in humans [5–8]. In mice, ablation of *Ufl1*, *Uba5*, or *Ufbp1* leads to impaired erythroid differentiation and embryonic lethality [9–11]. Additionally, neuron-specific knockout of either *Ufl1* or *Ddrgk1*

© 2026 Federation of American Societies for Experimental Biology.

(also known as *Ufbp1*) leads to marked neuronal loss and inflammation, highlighting their indispensable role in adult mouse mature neuronal survival [12]. Furthermore, mice with central nervous system (CNS)-specific *Ufm1* deletion exhibit neonatal lethality, microcephaly, and targeted neuronal apoptosis, which underscores the critical function of the UFM1 system in CNS development and homeostasis [8]. Beyond the nervous system and hematopoiesis, UFMylation is also required for the development and homeostasis of other tissues and organs [13–17]. For example, nephron tubule-specific *Ufl1*-knockout mice develop kidney atrophy and interstitial fibrosis [13]. Epithelial-specific deletion of *Ufl1* in mice disrupts UFMylation of Endothelin-1, which in turn elevates ET-1 expression and triggers skin pigmentation [14].

Tooth development relies on reciprocal epithelial-mesenchymal interactions, during which the dental epithelium differentiates into ameloblasts, the specialized cells that produce and mineralize enamel. This amelogenesis process is tightly regulated by multiple factors, and variants in genes encoding secreted enamel matrix proteins (*AMELX, ENAM, AMBN*), enamel matrix proteases (*MMP20, KLK4*), cell–cell and cell-matrix adhesion proteins (*LAMA3, LAMB3, COL17A1, ITGB6, AMTN, FAM83H*), transport proteins (*WDR72, SLC24A4*), as well as other genes such as *DLX3* and *FAM20A* have been linked to non-syndromic amelogenesis imperfecta [18], a congenital enamel defect. Enamel defects also occur in systemic disorders such as cleidocranial dysplasia (CCD), a rare genetic disorder characterized by skeletal abnormalities and dental anomalies. CCD is closely associated with mutations in the RUNX2 gene [19–21], a key transcription factor critical for bone and tooth development. *Runx2*$^{-/-}$ mice exhibit arrested tooth development at the bud stage and fail to deposit normal dentin and enamel matrices [22]. Epithelial-specific *Runx2* ablation via *K14-Cre* causes severe enamel mineralization defects and chalky-white teeth [23, 24]. Despite extensive studies on tooth development, the upstream regulatory mechanisms governing the expression and activity of these key regulatory molecules remain largely elusive.

Although UFMylation is critical for tissue development and homeostasis, its function in tooth development and amelogenesis remains unclear. In our previous study, we generated *K14-Cre*-mediated epithelial-specific *Ufl1* knockout mice for skin research [14]. Because *K14-Cre* also targets dental epithelium, the origin of ameloblasts, we also observed abnormal tooth morphology in these mice, suggesting a previously unrecognized role for UFL1 in dental development. Here, we utilized this mouse model to define the in vivo function and molecular mechanism of UFL1 in amelogenesis. We showed that loss of *Ufl1* in dental epithelial cells causes severe enamel hypoplasia and progressive tooth damage. Mechanistically, we demonstrated that UFL1-mediated UFMylation maintains amelogenesis by stabilizing RUNX2 protein, thereby uncovering a novel post-translational regulatory axis essential for mammalian enamel development.

2 | Material and Methods

2.1 | Animal Models

Ufl1$^{fx/fx}$ mice have been described previously [14]. *K14-Cre* mice were purchased from The Jackson Laboratory (Bar Harbor, ME, USA). The *Ufl1*-floxed mice were crossed with the *K14-Cre* mice to generate *Ufl1*$^{fx/+}$*; K14-Cre* mice, which were back-crossed with *Ufl1*$^{fx/fx}$ to produce *Ufl1*$^{fx/fx}$*; K14-Cre* (*Ufl1*$^{K14\text{-}Cre}$). Wild-type littermates were used as controls. Primer sequences for genotyping are shown in Table S1. The PCR bands for WT and alleles are 220 bp and 310 bp, respectively. The PCR bands for *K14-Cre* are 450 bp. The mice are on the C57BL/6 background and were reared in specific pathogen-free facilities. All of the available male *Ufl1*$^{K14\text{-}Cre}$ mice were randomly used for experiments ($n > 30$). All animal experiments were reviewed and approved by the Experimental Animal Ethics Committee of Hangzhou Normal University and were executed in strict compliance with the institution's guidelines for the care and use of laboratory animals.

2.2 | Stereomicroscopy, Methyl Red Staining, microCT

For stereomicroscopy of incisors, soft tissue was carefully dissected away from control and *Ufl1*$^{K14\text{-}Cre}$ mice using fine-tipped forceps under a stereomicroscope, followed by KOH treatment, and the intact incisors and alveolar bone were retained for stereomicroscopic observation. For methyl red staining, mandibular incisors were dissected from P10, P30, and P120 control and *Ufl1*$^{K14\text{-}Cre}$ mice, followed by careful removal of the attached bone and enamel organs. After removal of cellular debris from the exposed enamel surfaces, the incisors were incubated in methyl red working solution (4.5 mL 95% methanol mixed with 10 mg methyl red powder) at room temperature for 1–2 min, as previously described [25]. The specimens were then rinsed sequentially with 100% ethanol and double-distilled water, followed by air-drying at room temperature prior to observation. For microCT analysis, 2-month-old mice were euthanized first, and their skulls were dissected immediately and fixed in 4% paraformaldehyde, followed by processing according to standard protocols.

2.3 | Histology, Immunohistochemistry, Cell Apoptosis Assays

For histological analysis, mouse heads were fixed in 4% paraformaldehyde at 4°C overnight, followed by dehydration in a graded ethanol series, decalcification in 0.5 M EDTA (pH 7.4) at 37°C for 5–7 days, and embedding in paraffin wax. After deparaffinization and rehydration, 5-μm sections were subjected to hematoxylin and eosin (HE) or Masson's trichrome staining following standard protocols. All stained histological sections were observed and photographed using an upright microscope (Nikon ECLIPSE 80i, Nikon Corporation, Japan). For immunofluorescence, 5-μm sections were incubated overnight with primary antibodies against UFL1 (Bethyl Laboratories, A303-456A), Ki67 (Abcam, Ab15580), AMELX (Santa Cruz, sc365284), AMBN (biorbyt, orb155652), and RUNX2 (Santa Cruz, sc390351) at 4°C according to the manufacturers' instructions. Apoptosis was detected using the TUNEL BrightRed Apoptosis Detection Kit (Vazyme, Nanjing, China) following the manufacturer's instructions. Briefly, 5-μm paraffin-embedded sections were deparaffinized and rehydrated sequentially, washed with PBS, treated with 20 μg/mL proteinase K, and then incubated with the Labeling Mix and Recombinant TdT Enzyme.

15306860, 2026, 14, Downloaded from https://faseb.onlinelibrary.wiley.com/doi/10.1096/fj.202513068R by Xiao-Jing Zhu - Hangzhou Normal University , Wiley Online Library on [20/07/2026]. See the Terms and Conditions (https://onlinelibrary.wiley.com/terms-and-conditions) on Wiley Online Library for rules of use; OA articles are governed by the applicable Creative Commons License

The sections were counterstained with DAPI, mounted with anti-fade mounting medium, and subjected to fluorescence microscopic observation. Immunofluorescence and TUNEL images were captured with an upright research microscope (Leica DM4 B, Leica Microsystems, Germany).

2.4 | RNA Sequencing (RNA-Seq)

Enamel epithelium of P10 control and *Ufl1*$^{K14\text{-}Cre}$ mice ($n=3$ for each genotype) was subjected to RNA-Seq analysis by LC-Bio Technologies (Hangzhou, China). Briefly, mRNA was enriched from TRIzol-isolated total RNA via the oligo (dT) method. The enriched mRNA was fragmented and used for cDNA synthesis. After end repair and A-tailing, cDNA fragments were ligated to indexed adapters, followed by selection and amplification to generate the final sequencing library. Subsequently, 2×150 bp paired-end sequencing (PE150) was conducted on the Illumina NovaSeq 6000 platform. The clean reads were mapped onto the *Mus musculus* genome (mm10) using HISAT2, and the gene expression level in each sample was calculated with StringTie. Genes with a mean FPKM (fragments per kilobase of transcript per million fragments mapped) value <1 in both WT and *Ufl1*$^{K14\text{-}Cre}$ mice were excluded from subsequent analysis. Differential gene expression analysis was performed using DESeq2, and genes with $|\log2(FC)| >= 1$ and p-value <0.05 were defined as differentially expressed genes (DEGs) (Table S2, S3). The raw sequence data reported in this study have been deposited in the Genome Sequence Archive in the National Genomics Data Center, China National Center for Bioinformation/Beijing Institute of Genomics, Chinese Academy of Sciences, under accession number CRA035736, and are publicly accessible at https://bigd.big.ac.cn/gsa. Enrichment analysis of RNA-Seq data was performed using Enrichr [26, 27]. Bar Charts were generated using GraphPad Prism. The advanced volcano plot and heatmaps were constructed using the OmicStudio tools (https://www.omicstudio.cn/tool).

2.5 | Quantitative Reverse Transcription Polymerase Chain Reaction (qRT-PCR)

Total RNA was extracted from the enamel epithelium of P10 control and *Ufl1*$^{K14\text{-}Cre}$ mice using TRIzol reagent (Thermo Fisher Scientific, Waltham, MA, USA) and subsequently reverse-transcribed into cDNA using HiFiScript RT Master Mix (CWBIO, Taizhou, Jiangsu, China). QRT-PCR analysis was performed using UltraSYBR mixture (CWBIO) on the StepOnePlus Real-Time PCR System (Thermo Fisher Scientific). 18S rRNA was used as a reference gene. The $2^{-\Delta\Delta CT}$ method was used for the quantification of qRT–PCR data. Primer sequences were obtained from PrimerBank and are shown in Table S1. Data are represented as the mean ± SD. A p-value <0.05 was considered statistically significant.

2.6 | UFMylation Inhibition and ER Stress Rescue Assay

MC3T3-E1 cells were cultured in α-MEM medium supplemented with 10% fetal bovine serum and 1% penicillin–streptomycin (Procell, CM-0378) in a humidified incubator at 37°C with 5% CO_2. For drug treatment, cells were seeded in 6-well plates and incubated overnight to allow adhesion. At 60%–70% confluence, cells were divided into three groups: A control group treated with vehicle, a treatment group with 50 μM DKM2-93 (the UFMylation inhibitor; BBI, Shanghai, China), and a co-treatment group with 50 μM DKM2-93 and 300 μM tauroursodeoxycholic acid dihydrate (TUDCA, the ER stress inhibitor; BBI, Shanghai, China). After 48 h of incubation, cells were harvested and subjected to Western blot analysis to examine the expression levels of RUNX2. GAPDH was used as the loading control. Anti-RUNX2 (ABclonal, A11753) and anti-GAPDH (ABclonal, A19056) antibodies were used for immunoblotting.

2.7 | Co-Immunoprecipitation Assay and in Vivo UFMylation Assay

HEK293T cells were cultured in DMEM containing 10% FBS in a humidified incubator at 37°C with 5% CO_2. For the co-immunoprecipitation assay, cells were transfected with the indicated plasmids and harvested at 24 h post-transfection, followed by co-immunoprecipitation analysis using Anti-FLAG M2 magnetic beads (Sigma-Aldrich, St. Louis, MO, USA) as described previously [14]. Immunoprecipitates and input HEK293T cell lysates were resolved by SDS–PAGE and analyzed by Western blot. In vivo UFMylation assays were performed essentially as described previously [14]. Briefly, cells were harvested 36 h post-transfection, lysed by boiling in denaturing buffer to disrupt non-covalent interactions, diluted 20-fold, and incubated with Anti-FLAG M2 beads (Sigma-Aldrich). Immunoprecipitates and inputs were resolved by SDS-PAGE followed by western blot analysis. The antibodies used in this assay included anti-HA (Cell Signaling Technology, 3597S), anti-FLAG (Cell Signaling Technology, 3177S), anti-MYC (Proteintech, 16286–1-AP), and anti-UFM1 (Selleck, F3636).

2.8 | Statistics Analysis

The sample size was not predetermined by a statistical method. The experiments were not randomized. We cannot randomly allocate animals to experiment groups; rather, we relied on Mendelian inheritance to provide a natural randomization of the data. The investigators were not blind during experiments and outcome assessment. For quantification of diameter, surface length, and length of the lower incisors, these parameters were calculated from Micro-CT data ($n=3$). For quantification of cell proliferation and apoptosis, Ki67-positive cells and apoptotic cells in the labial cervical loop region were counted, respectively ($n=3$). For the quantification of Western blotting bands, relative protein expression levels were determined by normalizing the band intensity to that of GAPDH ($n=3$). All data were analyzed using GraphPad Prism software or Microsoft Excel and presented as mean ± SD. Experimental results' significance was evaluated by the Student's t-test. A p-value <0.05 was considered statistically significant.

3 | Results

3.1 | *Ufl1* Deletion Results in Amelogenesis Imperfecta in Mice

To investigate the consequences of *Ufl1* deficiency in tooth development, we generated conditional knockout mice of

15306860, 2026, 14, Downloaded from https://faseb.onlinelibrary.wiley.com/doi/10.1096/fj.202503068R by Xiao-Jing Zhu - Hangzhou Normal University , Wiley Online Library on [20/07/2026]. See the Terms and Conditions (https://onlinelibrary.wiley.com/terms-and-conditions) on Wiley Online Library for rules of use; OA articles are governed by the applicable Creative Commons License

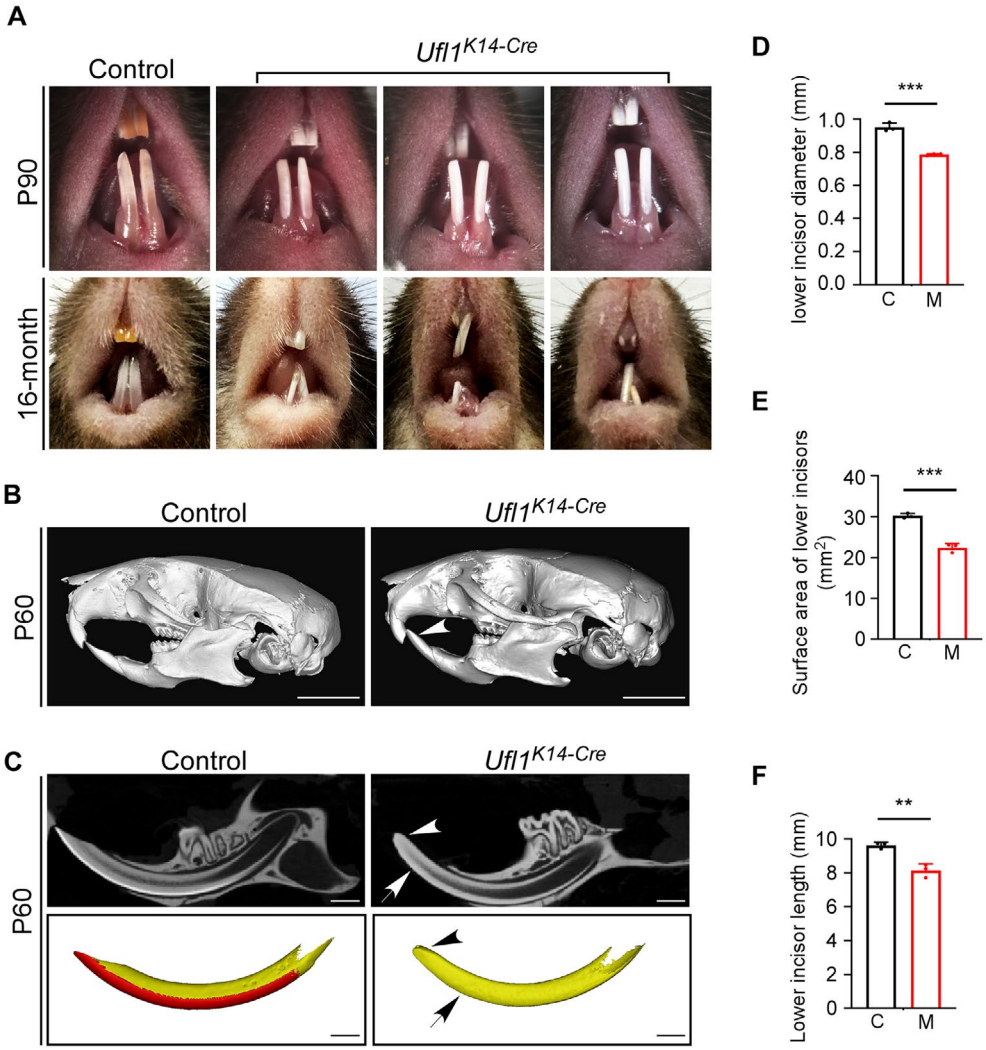


FIGURE 1 | Deletion of *Ufl1* in ectoderm-derived dental epithelium causes amelogenesis imperfecta in mice. (A) Frontal view of maxillary and mandibular incisors of control and $Ufl1^{K14\text{-}Cre}$ mice at P90 and 16 months of age. Control mice showed yellowish mineralized incisor enamel. $Ufl1^{K14\text{-}Cre}$ mice had chalky-white incisors with chipped edges at P90, and tooth wear, fracture, and loss were observed in 16-month-old mice. (B) MicroCT reconstructions of skulls from P60 control and $Ufl1^{K14\text{-}Cre}$ mice. Note that $Ufl1^{K14\text{-}Cre}$ mice exhibit blunt incisal edges (arrowhead). (C) Sagittal and three-dimensional microCT images reveal blunt incisal edges (arrowheads) and the absence of labial enamel in *Ufl1*-deficient incisors (arrows). (D–F) Statistical analyses show that the diameter, surface area, and length of the lower incisors in $Ufl1^{K14\text{-}Cre}$ are significantly reduced compared with those in control mice ($n = 3$). Data are presented as mean ± SD. $^{**}p < 0.01$, $^{***}p < 0.001$. Unpaired two-tailed Student's *t*-test (df = 4): D, t = 10.45; E, t = 11.26; F, t = 5.916. C, Control; M, $Ufl1^{K14\text{-}Cre}$. Scale bars: B, 5 mm; C, 1 mm.

Ufl1 in which *Ufl1* was specifically and efficiently ablated in epithelium-derived ameloblasts (Figure S1). We found that all male $Ufl1^{K14\text{-}Cre}$ mice examined exhibit amelogenesis imperfecta in both molars and incisors, whereas female $Ufl1^{K14\text{-}Cre}$ mice display normal tooth development at 2–3 months old. Morphological observation revealed that $Ufl1^{K14\text{-}Cre}$ mice displayed prominent chalky-white incisors with chipped edges at postnatal day 90 (P90) (Figure 1A). These defects were exacerbated in 16-month-old mice, characterized by severe tooth wear, fracture, and tooth loss (Figures 1A and S2). Notably, these phenotypes were already detectable as early as P30 (Fig. S3). Three-dimensional microCT reconstruction of skulls from 2-month-old $Ufl1^{K14\text{-}Cre}$ mice further confirmed incisors with chipped edges (Figure 1B,C). More importantly, microCT analysis demonstrated that the dental enamel layer, clearly visible in control mice, was completely absent in $Ufl1^{K14\text{-}Cre}$ mice (Figure 1C). Further quantitative analysis of microCT data revealed that the length, diameter, and surface area of the lower incisors in $Ufl1^{K14\text{-}Cre}$ mice were significantly reduced (Figure 1D–F).

3.2 | *Ufl1* Deficiency Impairs Enamel Deposition and Mineralization in Mice

To elucidate the underlying causes of tooth developmental abnormalities induced by *Ufl1* deficiency, we performed histological staining on mandibular incisors to assess enamel development. HE staining showed that enamel was deposited in $Ufl1^{K14\text{-}Cre}$ mice during postnatal development, but the enamel layer was significantly thinner than that in control mice (Figures 2A and S4). Immunofluorescence staining further revealed that the levels of key enamel matrix proteins (AMELX

15306860, 2026, 14, Downloaded from https://faseb.onlinelibrary.wiley.com/doi/10.1096/fj.202513068R by Xiao-Jing Zhu - Hangzhou Normal University , Wiley Online Library on [20/07/2026]. See the Terms and Conditions (https://onlinelibrary.wiley.com/terms-and-conditions) on Wiley Online Library for rules of use; OA articles are governed by the applicable Creative Commons License

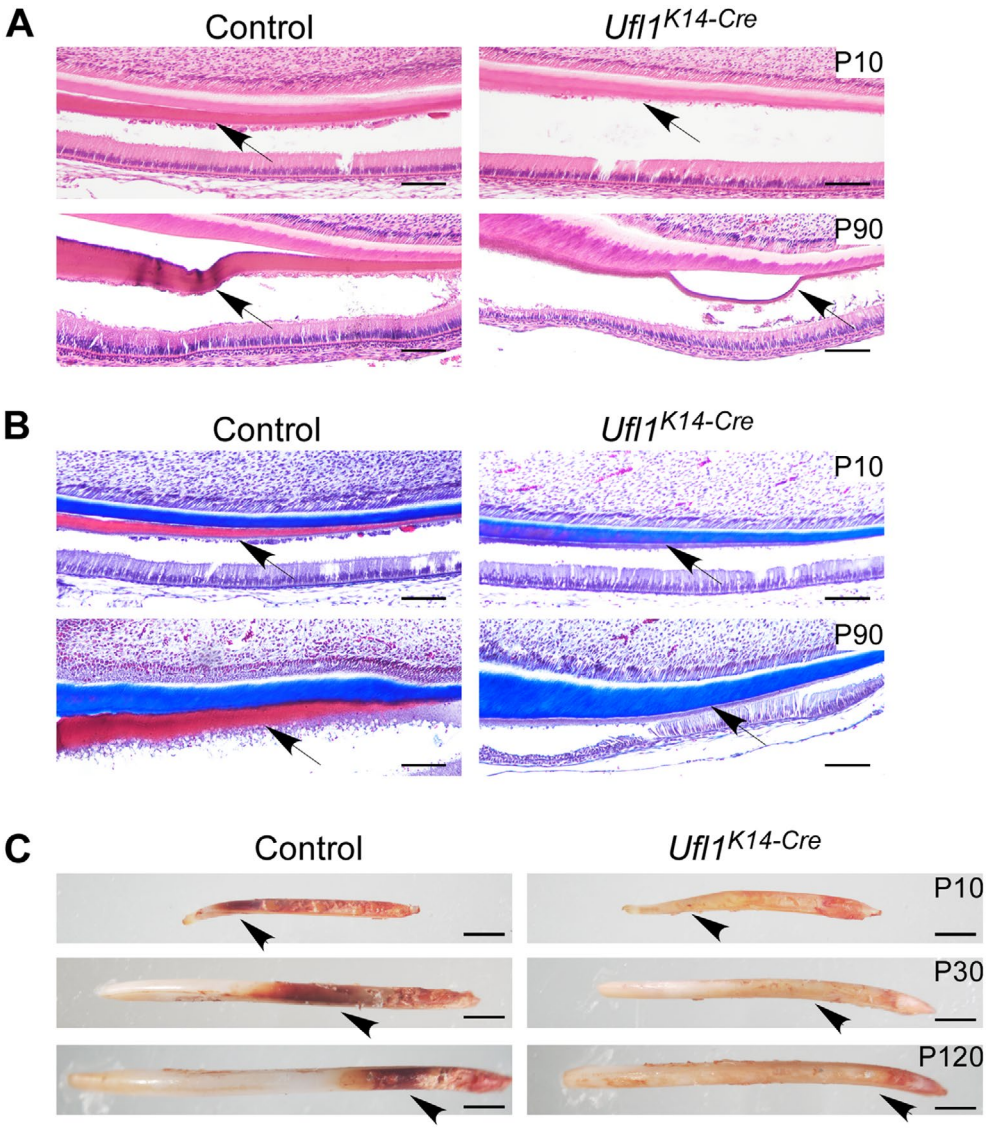


FIGURE 2 | Loss of epithelial *Ufl1* disrupts enamel matrix deposition and mineralization during tooth development. (A) HE staining of sagittal sections of incisors from control and $Ufl1^{K14\text{-}Cre}$ mice at P10 and P90. Note the thinned enamel matrix in $Ufl1^{K14\text{-}Cre}$ teeth (arrows). (B) Masson's trichrome staining of sagittal sections of incisors from control and $Ufl1^{K14\text{-}Cre}$ mice at P10 and P90. Note the absence of mineralized enamel in $Ufl1^{K14\text{-}Cre}$ teeth (arrows). (C) Methyl red staining showed that ameloblast regions exhibit deep red staining in control mice at P10, P30, and P120. In contrast, the staining was much fainter in $Ufl1^{K14\text{-}Cre}$ mice (arrowheads). Scale bars: A, B, 100 μm; C, 1 mm.

and AMBN) were markedly reduced in *Ufl1*-deficient ameloblasts at P0 (Fig. S5). These results suggest that enamel deposition is impaired, or alternatively, that enamel matrix proteins are prematurely degraded in the mutants. Masson's trichrome staining showed that the enamel of control mice was stained bright red, whereas no red staining was observed in the enamel of $Ufl1^{K14\text{-}Cre}$ mice (Figures 2B and S4), indicating a defect in enamel mineralization. Given that enamel mineralization depends on a specific pH microenvironment, an essential condition for ameloblasts to secrete hydrogen ions and promote enamel crystal mineralization [25], we evaluated pH changes in mandibular incisors using methyl red staining. The incisor enamel surfaces of control mice showed a dark orange-red stain, indicative of a highly acidic (low pH) environment. In contrast, the staining of $Ufl1^{K14\text{-}Cre}$ mice was pale yellow, reflecting a weakly acidic (high pH) environment (Figure 2C), suggesting that *Ufl1* deletion disrupts the acidic microenvironment required for normal enamel mineralization.

3.3 | Loss of *Ufl1* Leads to Abnormal Labial Cervical Loop Development in Mice

Given that the labial cervical loop (laCL) of incisors harbors stem cells that differentiate into ameloblasts, key cells responsible for enamel biosynthesis, we next investigated whether *Ufl1* deficiency perturbs labial cervical loop development. HE staining revealed a smaller and flattened laCL structure of $Ufl1^{K14\text{-}Cre}$ mandibular incisors compared with control mice (Figure 3A). Ki67 staining and TUNEL assay further demonstrated that *Ufl1* deletion resulted in a significant increase in cell proliferation and dramatically elevated apoptotic cell

15306860, 2026, 14, Downloaded from https://faseb.onlinelibrary.wiley.com/doi/10.1096/fj.202503068R by Xiao-Jing Zhu - Hangzhou Normal University , Wiley Online Library on [20/07/2026]. See the Terms and Conditions (https://onlinelibrary.wiley.com/terms-and-conditions) on Wiley Online Library for rules of use; OA articles are governed by the applicable Creative Commons License

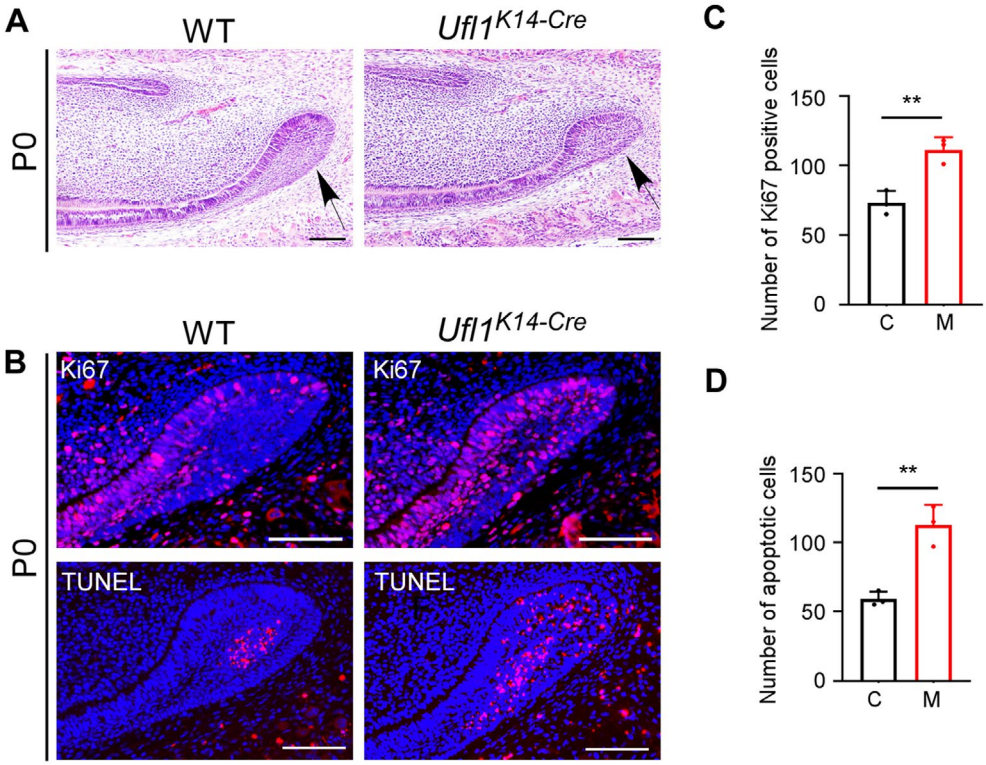


FIGURE 3 | *Ufl1* deficiency impairs labial cervical loop development in mice. (A) HE staining of sagittal sections of lower incisors from control and $Ufl1^{K14\text{-}Cre}$ mice at P0. The labial cervical loops of $Ufl1^{K14\text{-}Cre}$ exhibit a flattened morphology (arrow). (B) Immunofluorescence staining demonstrates a marked increase in Ki67-positive cell numbers and a significant elevation in apoptotic cell levels in the labial cervical loops of $Ufl1^{K14\text{-}Cre}$ mice. (C) Statistical analysis reveals a significant increase in the number of Ki67-positive cells in the labial cervical loops of $Ufl1^{K14\text{-}Cre}$ incisors compared with controls ($n = 3$). (D) Statistical analysis shows a dramatic increase in apoptotic cell numbers in the labial cervical loops of $Ufl1^{K14\text{-}Cre}$ incisors relative to controls ($n = 3$). Data are presented as mean ± SD. $^{**}p < 0.01$. Unpaired two-tailed Student's *t*-test (df = 4): C, t = 5.327; D, t = 5.971. C, Control; M, $Ufl1^{K14\text{-}Cre}$. Scale bars: 100 μm.

numbers in the laCL (Figure 3B–D). In sum, these results suggest that *Ufl1* is essential for the normal development of the laCL, and that dysregulation of cell proliferation and apoptosis within this structure may disrupt the proper differentiation of laCL-derived stem cells into functional ameloblasts, thus contributing to the enamel deposition and mineralization defects observed in $Ufl1^{K14\text{-}Cre}$ mice.

3.4 | *Ufl1*-Deficiency Causes Aberrant Gene Expression in Developing Ameloblasts

To further investigate the molecular mechanisms underlying UFL1-mediated amelogenesis, we performed RNA-Seq to profile gene expression in incisor ameloblasts from control and $Ufl1^{K14\text{-}Cre}$ mice at P10. A total of 234 upregulated and 266 downregulated DEGs were identified in $Ufl1^{K14\text{-}Cre}$ ameloblasts (Figure 4A). Next, we performed enrichment analysis using Enrichr [27].

Analysis against the Jensen_DISEASES_Curated gene sets revealed that downregulated DEGs were highly associated with amelogenesis imperfecta, dental enamel hypoplasia, and tooth hard tissue diseases (Figure 4B). GO_Molecular_function analysis showed that downregulated DEGs were most significantly enriched in gap junction channel activity and metal ion transmembrane transporter activity (Figure 4B), indicating that *Ufl1* deficiency disrupts intercellular communication via gap junctions and metal ion transmembrane transport. Notably, a panel of well-validated enamel deposition- and mineralization-related genes was significantly downregulated in *Ufl1*-deficient ameloblasts (Figure 4D), including several transcriptional targets of RUNX2, the master transcription factor orchestrating amelogenesis [24, 28–31]. This finding, together with the phenotypic similarity between our epithelial-specific *Ufl1* knockout mice and reported dental epithelial-specific *Runx2* knockout models [24], suggests that UFL1 regulates amelogenesis by modulating RUNX2 activity.

For upregulated DEGs, Chromatin immunoprecipitation enrichment analysis (ChEA) showed that upregulated DEGs were significantly enriched among target genes of the transcription factor TP53 (Figure 4C), a well-characterized tumor suppressor that plays a pivotal role in ER stress. Furthermore, enrichment analysis against WikiPathways demonstrated that upregulated DEGs were predominantly enriched in the unfolded protein response (Figure 4C). Consistent with these findings, genes involved in the response to ER stress, including *Bbc3, Bhlha15, Derl3, Ddit3, Hspa5, Hsp90b1, Hyou1, Manf, Pmaip1, Syvn1, Tmtc3*, and *Tnfrsf10b*, were significantly upregulated (Figure 4E). Finally, we validated a subset of DEGs via quantitative reverse transcription-PCR (qRT-PCR), and the results were consistent with the RNA-Seq data (Figure 4F). Taken together, our data demonstrate that *Ufl1* is essential for

15306860, 2026, 14, Downloaded from https://faseb.onlinelibrary.wiley.com/doi/10.1096/fj.202503068R by Xiao-Jing Zhu - Hangzhou Normal University , Wiley Online Library on [20/07/2026]. See the Terms and Conditions (https://onlinelibrary.wiley.com/terms-and-conditions) on Wiley Online Library for rules of use; OA articles are governed by the applicable Creative Commons License

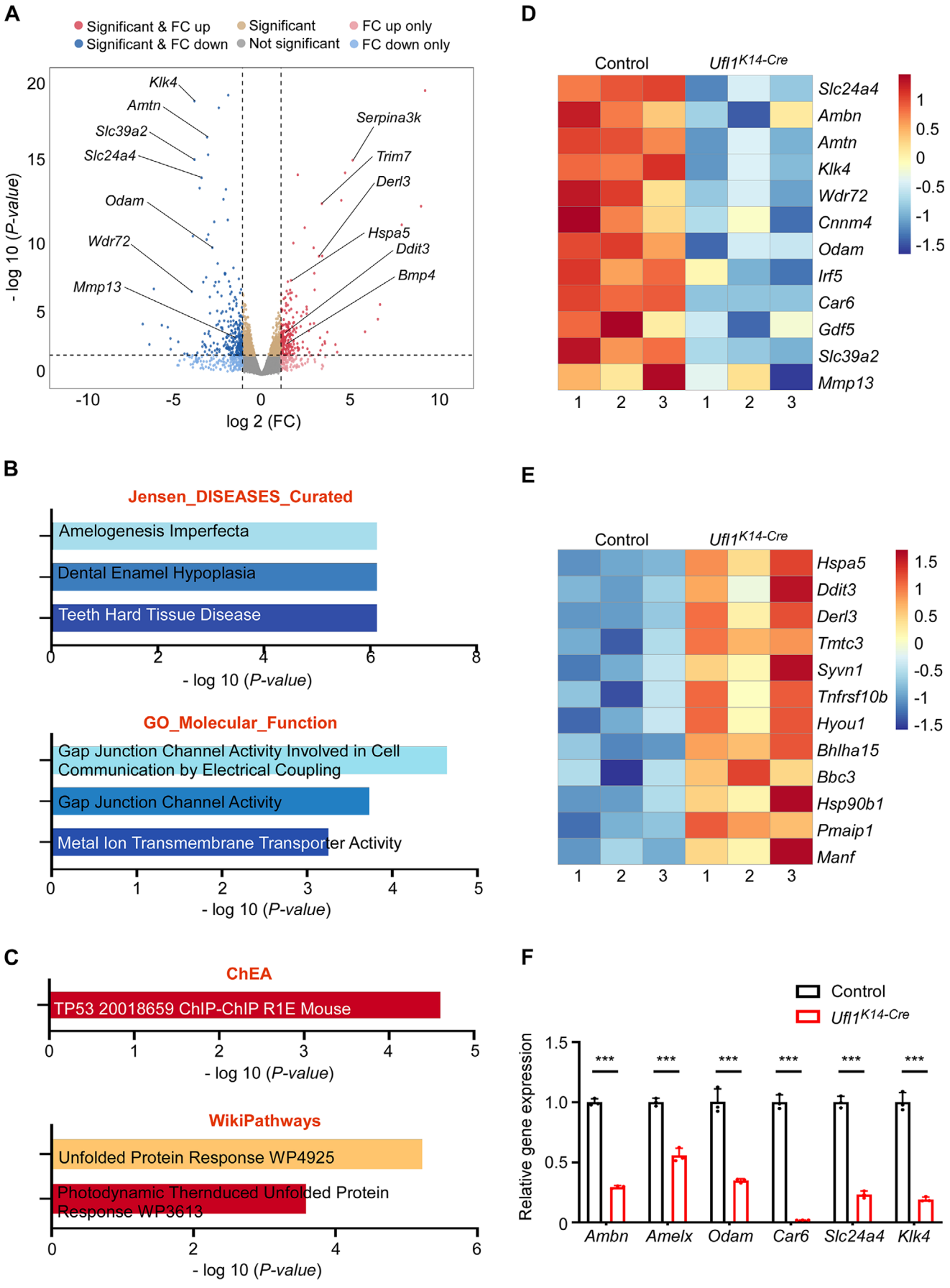


FIGURE 4 | Legend on next page.

15306860, 2026, 14, Downloaded from https://faseb.onlinelibrary.wiley.com/doi/10.1096/fj.202503068R by Xiao-Jing Zhu - Hangzhou Normal University , Wiley Online Library on [20/07/2026]. See the Terms and Conditions (https://onlinelibrary.wiley.com/terms-and-conditions) on Wiley Online Library for rules of use; OA articles are governed by the applicable Creative Commons License

FIGURE 4 | Dysregulated gene expression in ameloblasts of *Ufl1*-deficient incisors at P10. (A) Volcano plots of RNA-Seq data showing differential gene expression profiles in *Ufl1*-deficient ameloblasts. Annotated dots indicate representative DEGs. (B, C) Functional enrichment analyses of downregulated and upregulated DEGs, respectively. (D) Heatmap of representative upregulated DEGs related to tooth mineralization. (E) Heatmap of representative downregulated DEGs related to the response to ER stress. (F) Validation of RNA-Seq data by qRT-PCR for representative DEGs. Data are presented as mean ± SD. ***$p < 0.001$. Unpaired two-tailed Student's *t*-test (df = 4): *Ambn* t = 38.40; *Amelx* t = 11.26; *Odam* t = 10.44; *Car6* t = 27.78; *Slc24a4* t = 23.15; *Klk4* t = 17.18.

amelogenesis by regulating enamel matrix formation, mineralization, intercellular communication, and ER homeostasis in ameloblasts.

3.5 | *Ufl1* Deficiency Leads to the Degradation of RUNX2

Based on these findings, we hypothesized that RUNX2 is a direct downstream substrate of UFL1-mediated UFMylation during amelogenesis. To test this hypothesis, we first examined RUNX2 expression in *Ufl1*-deficient ameloblasts. Immunofluorescent staining results showed that RUNX2 protein level was significantly reduced in $Ufl1^{K14\text{-}Cre}$ ameloblasts at P0 and P10 (Figure 5A); however, its mRNA level was unchanged (Figure 5B). This dissociation between protein and mRNA expression indicated that UFL1 regulates RUNX2 at the post-translational level, consistent with the known function of UFMylation in controlling substrate protein stability. We next sought to validate whether RUNX2 is a direct substrate of the UFMylation pathway. Co-immunoprecipitation assays demonstrated that RUNX2 interacts with the key UFMylation proteins UFL1 and DDRGK1 (Figure 5C). To directly confirm covalent UFM1 conjugation to RUNX2, we performed in vivo UFMylation assays in HEK293T cells co-expressing RUNX2 and all core UFMylation cascade components UBA5, UFC1, UFL1, UFM1, and DDRGK1. The results showed that RUNX2 was modified by the active UFM1ΔC2 variant, which carries an exposed C-terminal glycine 83 residue. In contrast, the catalytically inactive UFM1ΔC3 mutant, which lacks this critical glycine residue, failed to mediate UFM1 conjugation to RUNX2 (Figure 5D).

To further confirm the causal link between UFMylation and RUNX2 stability, we treated MC3T3-E1 cells with DKM2-93, a selective pharmacological inhibitor of UFMylation. Inhibition of UFMylation significantly reduced endogenous RUNX2 protein levels in MC3T3-E1 cells (Figure 5E). Given that our RNA-Seq data revealed a robust ER stress response in *Ufl1*-deficient ameloblasts, we next tested whether RUNX2 downregulation arises as a secondary consequence of ER stress induced by UFMylation inhibition. To this end, we performed a rescue assay with TUDCA, a well-characterized ER stress inhibitor. We found that TUDCA failed to restore RUNX2 protein levels in DKM2-93-treated cells (Figure 5E). Collectively, these findings demonstrate that RUNX2 is a novel substrate of UFL1-mediated UFMylation, and that UFMylation is essential for maintaining RUNX2 protein stability, thereby governing the transcriptional program of enamel matrix mineralization during amelogenesis.

4 | Discussion

Amelogenesis imperfecta is a group of inherited dental disorders characterized by defective enamel formation, severely impacting oral health due to enamel hypoplasia, hypomineralization, and increased tooth fragility. In this study, we explored the role of UFL1, the sole E3 ligase in the UFMylation pathway, in mammalian amelogenesis. Our findings reveal that epithelial-specific *Ufl1* deletion induces amelogenesis imperfecta-like phenotypes in mice, demonstrating UFL1 as a critical regulator of mammalian amelogenesis. Furthermore, we identify RUNX2 as a novel substrate of UFL1-mediated UFMylation, and show that UFMylation regulates amelogenesis by modulating RUNX2 protein stability.

RUNX2 is a critical transcription factor orchestrating bone and tooth development, and its expression is tightly regulated at multiple levels. Transcriptionally, the *Runx2* P1 promoter is specifically bound and activated by DLX5, while MSX2 represses its expression by binding to the same regulatory region [32]. Post-transcriptionally, RUNX2 protein levels can be influenced by m^6A modification of its mRNA and microRNA [33]. At the post-translational level, multiple modifications, including phosphorylation, acetylation, SUMOylation, and glycosylation, precisely modulate RUNX2 protein activity and stability [34]. Here, we identify UFL1-mediated UFMylation as a novel post-translational layer regulating RUNX2 in amelogenesis, expanding this complex regulatory network. Notably, our study identifies a sex-specific role for UFL1-mediated UFMylation in enamel development, with *Ufl1* deletion leading to reduced enamel only in male mice. Previous studies have revealed the mutual transactivational repression between the androgen receptor (AR) and RUNX2: AR, activated by androgens, inhibits the transcriptional activity of RUNX2 [35, 36]. Importantly, a prior study in rats has documented high AR expression in maturation-stage ameloblasts [37]. In mice, the AR protein is readily detected in maturation-stage ameloblasts and exhibits clear nuclear localization [38]. At the transcript level, mouse *AR* expression is independently validated by both our ameloblast RNA-seq data presented in this manuscript and the public NCBI GEO dataset (GSE57224). Thus, we propose that loss of UFL1 exacerbates AR-dependent repression of RUNX2, impairing ameloblast function and enamel formation in males. Our findings thus suggest UFL1-UFMylation as a new regulatory mechanism in AR-RUNX2 crosstalk, which specifically protects enamel development in males by maintaining RUNX2 activity under active androgen signaling.

In addition to defective enamel mineralization, our study identified other pathological changes in *Ufl1*-deficient mice that may also contribute to the observed enamel defects. Specifically, we found that LaCL, a specialized niche containing dental epithelial

15306860, 2026, 14, Downloaded from https://faseb.onlinelibrary.wiley.com/doi/10.1096/fj.202503068R by Xiao-Jing Zhu - Hangzhou Normal University , Wiley Online Library on [20/07/2026]. See the Terms and Conditions (https://onlinelibrary.wiley.com/terms-and-conditions) on Wiley Online Library for rules of use; OA articles are governed by the applicable Creative Commons License

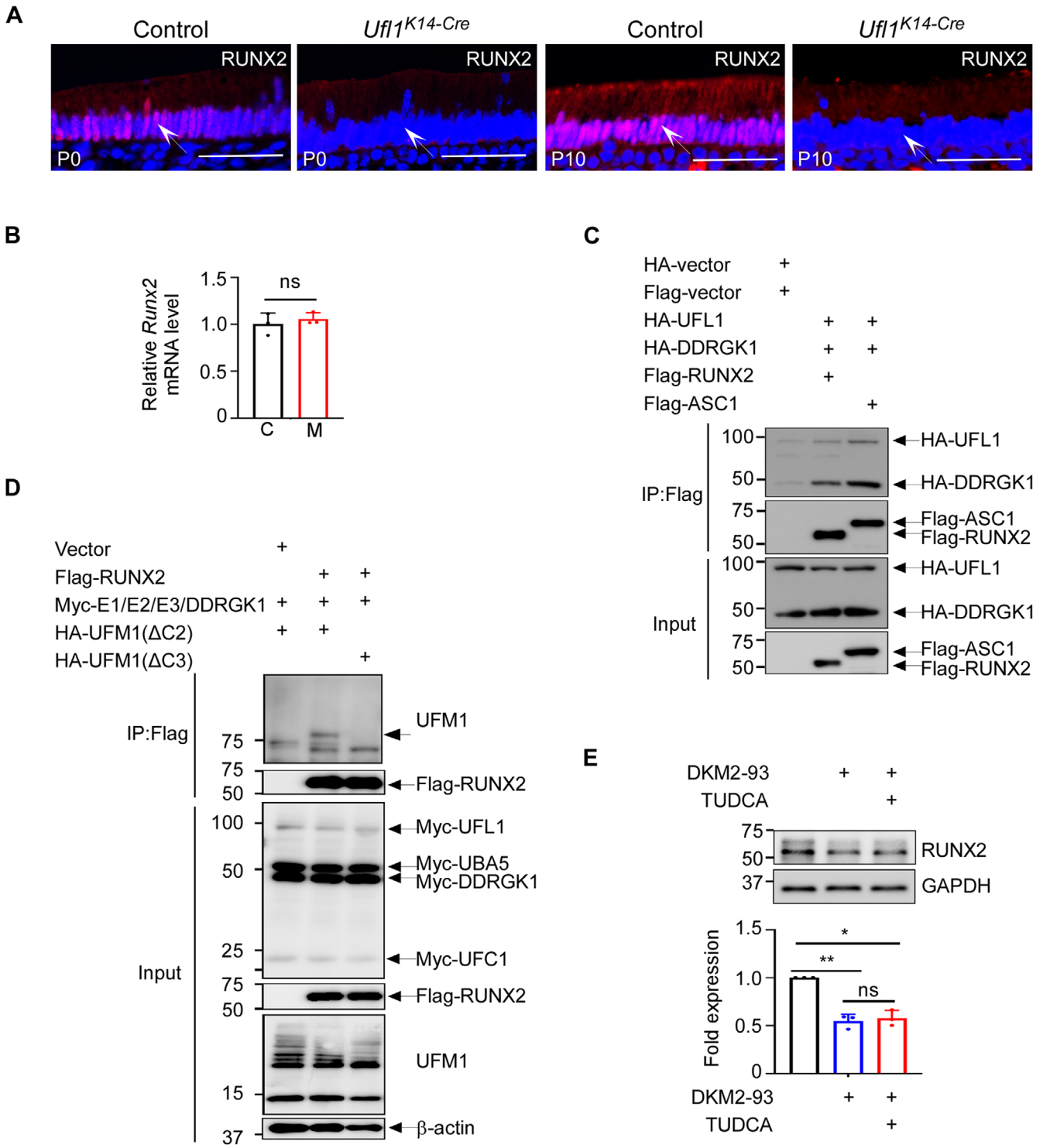


FIGURE 5 | UFL1 interacts with RUNX2 and modulates its protein expression during tooth development. (A) Immunofluorescence staining showing a marked decrease in RUNX2 expression (arrows) in ameloblasts of *Ufl1* $^{K14\text{-}Cre}$ mice at P0 and P10. (B) *Runx2* mRNA levels were not significantly altered in ameloblasts of *Ufl1*-deficient mice at P10. (C) Co-immunoprecipitation assays followed by Western blot analysis demonstrated interactions between UFL1, DDRGK1, and RUNX2 in HEK293T cells. Cells were transfected with the indicated vectors and harvested for Co-immunoprecipitation analysis at 36 h post-transfection. (D) UFMylation of RUNX2 was analyzed by western blot with anti-UFM1 antibody in HEK293T cells expressing the UFMylation system components. (E) Western blot detection of RUNX2 in MC3T3-E1 cells. Cells were treated with vehicle (control), 50 μM DKM2-93, or 50 μM DKM2-93 plus 300 μM TUDCA for 48 h. GAPDH was used as a loading control. The expression of RUNX2 protein level was determined by normalizing its gray value to that of GAPDH. Data are presented as mean ± SD. *$p < 0.05$, **$p < 0.01$. B, Unpaired two-tailed Student's *t*-test, df = 4, t = 0.697; 4; E, Paired two-tailed Student's *t*-test (df = 2), control vs. DKM2-93, t = 10.95; control vs. DKM2-93 + TUDCA, t = 8.853; DKM2-93 vs. DKM2-93 + TUDCA, t = 0.547. Scale bars: 50 μm.

15306860, 2026, 14, Downloaded from https://faseb.onlinelibrary.wiley.com/doi/10.1096/fj.202503068R by Xiao-Jing Zhu - Hangzhou Normal University , Wiley Online Library on [20/07/2026]. See the Terms and Conditions (https://onlinelibrary.wiley.com/terms-and-conditions) on Wiley Online Library for rules of use; OA articles are governed by the applicable Creative Commons License

stem cells (DESC) essential for sustaining ameloblast generation and differentiation, exhibited abnormal development in *Ufl1*$^{K14\text{-}Cre}$ mice. SOX2 maintains DESC pluripotency in the LaCL to support continuous incisor growth and guide ameloblast lineage commitment [39]. Alongside the abnormal LaCL development, our unpublished data show reduced SOX2 expression in *Ufl1*-deficient incisors. Given the critical role of SOX2, its downregulation is likely to impair long-term ameloblast renewal and differentiation ability, further contributing to the enamel defects in *Ufl1*-deficient mice. However, our co-immunoprecipitation assays failed to detect a direct interaction between SOX2 and UFL1, thus excluding SOX2 as a direct UFMylation substrate. Intriguingly, the enamel phenotypes in *Ufl1*$^{K14\text{-}Cre}$ mice are more severe than those reported in ameloblast-specific *Runx2* conditional knockout models. This phenotypic difference, together with the LaCL defects, suggests that *Ufl1* regulates amelogenesis through broader mechanisms beyond just directly stabilizing RUNX2.

In sum, our study uncovers a novel role of UFL1-mediated UFMylation in enamel development, advances our understanding of the post-translational control of key transcription factors in amelogenesis, and offers a novel animal model for amelogenesis imperfecta. However, we have not yet identified the specific molecular mechanism by which UFMylation regulates RUNX2, including its precise UFMylation sites, and these will be investigated in future studies.

Author Contributions

D. Liu, contributed to design, data acquisition, analysis, and interpretation, drafted and critically revised the manuscript; L. Chen, contributed to data acquisition and analysis, drafted and critically revised the manuscript; H. Xu, contributed to data acquisition and analysis, and critically revised the manuscript; X. Yang, K. Wang, contributed to design, and critically revised the manuscript; M. Wang, contributed to conception, design, and critically revised the manuscript. X.-J. Zhu, contributed to conception, design, data interpretation, drafted, and critically revised the manuscript. All authors gave final approval and agreed to be accountable for all aspects of the work.

Funding

This work was supported by the Zhejiang Provincial Natural Science Foundation of China (Grant No. LMS26H140004).

Ethics Statement

All animal experiments were reviewed and approved by the Experimental Animal Ethics Committee of Hangzhou Normal University.

Conflicts of Interest

The authors declare no conflicts of interest.

Data Availability Statement

The data that support the findings of this study are openly available in the GSA at https://bigd.big.ac.cn/gsa, reference number CRA035736.

References

1. X. Zhou, S. J. Mahdizadeh, M. Le Gallo, L. A. Eriksson, E. Chevet, and E. Lafont, "UFMylation: A Ubiquitin-Like Modification," *Trends in Biochemical Sciences* 49 (2024): 52–67.

2. R. N. Wang, L. Li, J. Zhou, and J. Ran, "Multifaceted Roles of UFMylation in Health and Disease," *Acta Pharmacologica Sinica* 46 (2025): 805–815.

3. M. Komatsu, T. Chiba, K. Tatsumi, et al., "A Novel Protein-Conjugating System for Ufm1, a Ubiquitin-Fold Modifier," *EMBO Journal* 23 (2004): 1977–1986.

4. M. Komatsu, T. Inada, and N. N. Noda, "The UFM1 System: Working Principles, Cellular Functions, and Pathophysiology," *Molecular Cell* 84 (2024): 156–169.

5. Y. Han, Y. Ge, H. Liu, et al., "A Novel Compound Heterozygous Mutation of UFC1 in a Patient With Neurodevelopmental Disorder," *Genes & Genomics* 46 (2024): 1037–1043.

6. E. M. C. Hamilton, E. Bertini, L. Kalaydjieva, et al., "UFM1 Founder Mutation in the Roma Population Causes Recessive Variant of H-ABC," *Neurology* 89 (2017): 1821–1828.

7. M. S. Nahorski, S. Maddirevula, R. Ishimura, et al., "Biallelic UFM1 and UFC1 Mutations Expand the Essential Role of Ufmylation in Brain Development," *Brain* 141 (2018): 1934–1945.

8. M. Muona, R. Ishimura, A. Laari, et al., "Biallelic Variants in UBA5 Link Dysfunctional UFM1 Ubiquitin-Like Modifier Pathway to Severe Infantile-Onset Encephalopathy," *American Journal of Human Genetics* 99 (2016): 683–694.

9. Y. Cai, W. Pi, S. Sivaprakasam, et al., "UFBP1, a Key Component of the Ufm1 Conjugation System, Is Essential for Ufmylation-Mediated Regulation of Erythroid Development," *PLoS Genetics* 11 (2015): e1005643.

10. K. Tatsumi, H. Yamamoto-Mukai, R. Shimizu, et al., "The Ufm1-Activating Enzyme Uba5 Is Indispensable for Erythroid Differentiation in Mice," *Nature Communications* 2 (2011): 181.

11. M. Zhang, X. Zhu, Y. Zhang, et al., "RCAD/Ufl1, a Ufm1 E3 Ligase, Is Essential for Hematopoietic Stem Cell Function and Murine Hematopoiesis," *Cell Death and Differentiation* 22 (2015): 1922–1934.

12. J. Zhang, H. Zhu, S. Liu, et al., "Deficiency of Murine UFM1-Specific E3 Ligase Causes Microcephaly and Inflammation," *Molecular Neurobiology* 59 (2022): 6363–6372.

13. Y. Zhou, X. Ye, C. Zhang, et al., "Ufl1 Deficiency Causes Kidney Atrophy Associated With Disruption of Endoplasmic Reticulum Homeostasis," *Journal of Genetics and Genomics* 48 (2021): 403–410.

14. K. Wang, H. N. Xu, Y. W. Wang, et al., "Ufl1 Deficiency Causes Skin Pigmentation by Up-Regulation of Endothelin-1," *Frontiers in Cell and Development Biology* 10 (2022): 961675.

15. J. Li, G. Yue, W. Ma, et al., "Ufm1-Specific Ligase Ufl1 Regulates Endoplasmic Reticulum Homeostasis and Protects Against Heart Failure," *Circulation: Heart Failure* 11 (2018): e004917.

16. M. Weisz-Hubshman, A. T. Egunsula, B. Dawson, et al., "DDRGK1 Is Required for the Proper Development and Maintenance of the Growth Plate Cartilage," *Human Molecular Genetics* 31 (2022): 2820–2830.

17. R. Yang, H. Wang, B. Kang, et al., "CDK5RAP3, a UFL1 Substrate Adaptor, Is Crucial for Liver Development," *Development* 146 (2019): dev169235.

18. C. E. L. Smith, J. A. Poulter, A. Antanaviciute, et al., "Amelogenesis Imperfecta; Genes, Proteins, and Pathways," *Frontiers in Physiology* 8 (2017): 435.

19. S. Ogawa, S. Higuchi, Y. Yoshimoto, et al., "Functional Impact of Pathogenic Mutations in the Runt Homology Domain of Mouse Runx2 on Skeletal and Dental Phenotypes in Cleidocranial Dysplasia," *Journal of Bone and Mineral Research* (2025): zjaf201.

20. L. Dalle Carbonare, A. Minoia, A. Gandini, et al., "Unraveling RUNX2 Mutation in a Cleidocranial Dysplasia Patient: Molecular Insights Into Osteogenesis and Proteostasis," *Genes Dis* 12 (2025): 101449.

15306860, 2026, 14, Downloaded from https://faseb.onlinelibrary.wiley.com/doi/10.1096/fj.202601306R by Xiao-Jing Zhu - Hangzhou Normal University , Wiley Online Library on [20/07/2026]. See the Terms and Conditions (https://onlinelibrary.wiley.com/terms-and-conditions) on Wiley Online Library for rules of use; OA articles are governed by the applicable Creative Commons License

21. S. Thaweesapphithak, J. Saengsin, W. Kamolvisit, T. Theerapanon, T. Porntaveetus, and V. Shotelersuk, "Cleidocranial Dysplasia and Novel RUNX2 Variants: Dental, Craniofacial, and Osseous Manifestations," *Journal of Applied Oral Science* 30 (2022): e20220028.

22. R. N. D'Souza, T. Aberg, J. Gaikwad, et al., "Cbfa1 Is Required for Epithelial-Mesenchymal Interactions Regulating Tooth Development in Mice," *Development* 126 (1999): 2911–2920.

23. Y. Tian, H. Mu, Z. Dong, et al., "The Synergistic Effects of TGF-beta1 and RUNX2 on Enamel Mineralization Through Regulating ODAPH Expression During the Maturation Stage," *Journal of Molecular Histology* 53 (2022): 483–492.

24. Q. Chu, Y. Gao, X. Gao, et al., "Ablation of Runx2 in Ameloblasts Suppresses Enamel Maturation in Tooth Development," *Scientific Reports* 8 (2018): 9594.

25. S. K. Wang, Y. Hu, J. Yang, et al., "Critical Roles for WDR72 in Calcium Transport and Matrix Protein Removal During Enamel Maturation," *Molecular Genetics & Genomic Medicine* 3 (2015): 302–319.

26. M. V. Kuleshov, M. R. Jones, A. D. Rouillard, et al., "Enrichr: A Comprehensive Gene Set Enrichment Analysis Web Server 2016 Update," *Nucleic Acids Research* 44 (2016): W90–W97.

27. Z. Xie, A. Bailey, M. V. Kuleshov, et al., "Gene Set Knowledge Discovery With Enrichr," *Current Protocols* 1 (2021): e90.

28. S. Dhamija and P. H. Krebsbach, "Role of Cbfa1 in Ameloblastin Gene Transcription," *Journal of Biological Chemistry* 276 (2001): 35159–35164.

29. H. K. Lee, D. S. Lee, H. M. Ryoo, et al., "The Odontogenic Ameloblast-Associated Protein (ODAM) Cooperates With RUNX2 and Modulates Enamel Mineralization via Regulation of MMP-20," *Journal of Cellular Biochemistry* 111 (2010): 755–767.

30. X. Liu, Y. Wang, L. Zhang, et al., "Combination of Runx2 and Cbf-beta Upregulates Amelotin Gene Expression in Ameloblasts by Directly Interacting With Cis-Enhancers During Amelogenesis," *Molecular Medicine Reports* 17 (2018): 6068–6076.

31. X. Liu, C. Xu, Y. Tian, et al., "RUNX2 Contributes to TGF-beta1-Induced Expression of Wdr72 in Ameloblasts During Enamel Mineralization," *Biomedicine & Pharmacotherapy* 118 (2019): 109235.

32. M. H. Lee, Y. J. Kim, W. J. Yoon, et al., "Dlx5 Specifically Regulates Runx2 Type II Expression by Binding to Homeodomain-Response Elements in the Runx2 Distal Promoter," *Journal of Biological Chemistry* 280 (2005): 35579–35587.

33. X. Sun, X. Meng, Y. Piao, S. Dong, and Q. Dong, "METTL3 Promotes Osteogenic Differentiation of Human Periodontal Ligament Stem Cells Through IGF2BP1-Mediated Regulation of Runx2 Stability," *International Journal of Medical Sciences* 21 (2024): 664–673.

34. K. Gomathi, N. Akshaya, N. Srinaath, A. Moorthi, and N. Selvamurugan, "Regulation of Runx2 by Post-Translational Modifications in Osteoblast Differentiation," *Life Sciences* 245 (2020): 117389.

35. H. Kawate, Y. Wu, K. Ohnaka, and R. Takayanagi, "Mutual Transactivational Repression of Runx2 and the Androgen Receptor by an Impairment of Their Normal Compartmentalization," *Journal of Steroid Biochemistry and Molecular Biology* 105 (2007): 46–56.

36. S. K. Baniwal, O. Khalid, D. Sir, G. Buchanan, G. A. Coetzee, and B. Frenkel, "Repression of Runx2 by Androgen Receptor (AR) in Osteoblasts and Prostate Cancer Cells: AR Binds Runx2 and Abrogates Its Recruitment to DNA," *Molecular Endocrinology* 23 (2009): 1203–1214.

37. S. Houari, S. Loiodice, K. Jedeon, A. Berdal, and S. Babajko, "Expression of Steroid Receptors in Ameloblasts During Amelogenesis in Rat Incisors," *Frontiers in Physiology* 7 (2016): 503.

38. M. H. Le, Y. Nakano, D. Abduweli Uyghurturk, L. Zhu, and P. K. Den Besten, "Fluoride Alters Klk4 Expression in Maturation Ameloblasts Through Androgen and Progesterone Receptor Signaling," *Frontiers in Physiology* 8 (2017): 925.

39. Z. Sun, W. Yu, M. Sanz Navarro, et al., "Sox2 and Lef-1 Interact With Pitx2 to Regulate Incisor Development and Stem Cell Renewal," *Development* 143 (2016): 4115–4126.

Supporting Information

Additional supporting information can be found online in the Supporting Information section. **Figure S1:** Characterization of *Ufl1*$^{K14\text{-}Cre}$ conditional knockout mice. (A) Genotyping of *Ufl1*$^{fx/fx}$ and control mice by PCR. The PCR bands for WT and *Ufl1*$^{fx/fx}$ alleles are 220 bp and 310 bp, respectively. Mice homozygous for the floxed *Ufl1* allele and positive for the *K14-Cre* transgene are designated as *Ufl1*$^{K14\text{-}Cre}$. (B) qRT-PCR analysis of relative *Ufl1* gene expression in ameloblasts from *Ufl1* $^{K14\text{-}Cre}$ and WT control mice at P10.18S was used as an internal control. Data are presented as mean ± SD ($n = 3$). Unpaired two-tailed Student's *t*-test: df = 4, t = 27.72, $^{**}p < 0.001$. (C) Immunofluorescence staining of UFL1 in the dental enamel epithelium of *Ufl1*$^{K14\text{-}Cre}$ and control mice at P0. Arrows indicate decreased UFL1 expression in *Ufl1*$^{K14\text{-}Cre}$ mice compared with controls. Scale bar, 100 μm. **Figure S2:** *Ufl1*$^{K14\text{-}Cre}$ mice exhibit severe dental damage in old age. (A–D) Incisors from control mice maintained intact morphology with sharp incisal edges. In contrast, Ufl1-deficient mice displayed blunt incisal edges (arrows), accompanied by marked and severe incisor wear (arrowheads) at 16 months of age. Scale bars: 500 μm. **Figure S3:** Apparent tooth wear and enamel chalkiness in Ufl1-deficient mice as early as P30. (A) Frontal views of maxillary and mandibular incisors from control and *Ufl1*$^{K14\text{-}Cre}$ incisors at P30. The *Ufl1*$^{K14\text{-}Cre}$ mice exhibited incisors with a distinct chalky appearance compared with control mice. (B) Lateral views of the mandibular incisors of control and *Ufl1*$^{K14\text{-}Cre}$ mice at P30. Incisal edges of control mice were sharp, whereas those of Ufl1-deficient mice were blunt (arrowheads). Scale bars: 1 mm. **Figure S4:** Loss of epithelial Ufl1 disrupts enamel matrix deposition and mineralization at P0. (A, B) HE staining of sagittal sections of incisors from control and *Ufl1*$^{K14\text{-}Cre}$ mice at P0. Note the thinned enamel matrix in *Ufl1*$^{\text{K14-Cre}}$ teeth (arrows). (C, D) Masson's trichrome staining of sagittal sections of incisors from control and *Ufl1*$^{\text{K14-Cre}}$ mice at P0. Note the absence of mineralized enamel in *Ufl1*$^{\text{K14-Cre}}$ teeth (arrows). Scale bars: 100 μm. **Figure S5:** Immunofluorescence analysis reveals markedly decreased AMELX (A, B) and AMBN (C, D) protein levels in Ufl1-deficient ameloblasts relative to controls at P0 (arrows). Scale bars: 50 μm. **Table S1:** Nucleotide sequences of primers used in genotyping (#) and quantitative real-time PCR. **Table S2:** Up-regulated differentially expressed transcripts in control and *Ufl1*$^{K14\text{-}Cre}$ ameloblasts at P10. **Table S3:** Down-regulated differentially expressed transcripts in control and *Ufl1*$^{K14\text{-}Cre}$ ameloblasts at P10.

15306860, 2026, 14, Downloaded from https://faseb.onlinelibrary.wiley.com/doi/10.1096/fj.202503068R by Xiao-Jing Zhu - Hangzhou Normal University , Wiley Online Library on [20/07/2026]. See the Terms and Conditions (https://onlinelibrary.wiley.com/terms-and-conditions) on Wiley Online Library for rules of use; OA articles are governed by the applicable Creative Commons License